



THE UNIVERSITY *of* EDINBURGH

Edinburgh Research Explorer

## PET-MRI of coronary artery disease

### Citation for published version:

Whittington, B, Dweck, MR, van Beek, EJR, Newby, DE & Williams, MC 2022, 'PET-MRI of coronary artery disease', *Journal of Magnetic Resonance Imaging*.

### Link:

[Link to publication record in Edinburgh Research Explorer](#)

### Document Version:

Publisher's PDF, also known as Version of record

### Published In:

Journal of Magnetic Resonance Imaging

### General rights






Copyright for the publications made accessible via the Edinburgh Research Explorer is retained by the author(s) and / or other copyright owners and it is a condition of accessing these publications that users recognise and abide by the legal requirements associated with these rights.

### Take down policy

The University of Edinburgh has made every reasonable effort to ensure that Edinburgh Research Explorer content complies with UK legislation. If you believe that the public display of this file breaches copyright please contact [openaccess@ed.ac.uk](mailto:openaccess@ed.ac.uk) providing details, and we will remove access to the work immediately and investigate your claim.



# PET-MRI of Coronary Artery Disease

Beth Whittington, MD,<sup>1,2</sup>  Marc R. Dweck, MBChB, PhD,<sup>1,2</sup>   
Edwin J.R. van Beek, MD, PhD,<sup>2</sup>  David Newby, DM, PhD,<sup>1,2</sup>  and  
Michelle C. Williams, MBChB, PhD<sup>1,2\*</sup> 

Simultaneous positron emission tomography and magnetic resonance imaging (PET-MRI) combines the anatomical detail and tissue characterization of MRI with the functional information from PET. Within the coronary arteries, this hybrid technique can be used to identify biological activity combined with anatomically high-risk plaque features to better understand the processes underlying coronary atherosclerosis. Furthermore, the downstream effects of coronary artery disease on the myocardium can be characterized by providing information on myocardial perfusion, viability, and function. This review will describe the current capabilities of PET-MRI in coronary artery disease and discuss the limitations and future directions of this emerging technique.

**Level of Evidence:** 5

**Technical Efficacy:** Stage 3

J. MAGN. RESON. IMAGING 2022.

Atherosclerosis remains the leading cause of morbidity and mortality worldwide. Coronary artery disease (CAD) is the commonest clinical manifestation of atherosclerotic disease and remains the largest single cause of death.<sup>1</sup> Historically, imaging has focused on assessment of coronary artery stenoses and the associated ischemia. However, post-mortem studies have shown that over 70% of myocardial infarctions are attributable to atherosclerotic plaques that cause less than 50% luminal stenosis. These non-obstructive culprit plaques have pathological features which are associated with an increased likelihood of initiating an acute event.<sup>2</sup> This has led to the development of imaging modalities that can identify these high-risk plaque features and potentially predict future effects.

Cardiac magnetic resonance (CMR) imaging is a versatile non-invasive technique that provides multi-parametric assessment of cardiac function, tissue viability, and cardiac anatomy in a single examination. Its development over the past 40 years has led to CMR becoming a key imaging tool for the diagnosis and management of CAD. Recently the diagnostic capabilities of combined CMR and positron emission tomography (PET) have been explored, with the development of hybrid PET-MRI scanners. This enables the combination of the anatomical detail and tissue

characterization of MRI with the functional information from PET, to enable in vivo assessment of cardiac physiology at a molecular level.<sup>3</sup>

This review will explore the use of combined positron emission tomography (PET) and magnetic resonance imaging (MRI) in CAD (Table 1).

## Capabilities of PET-MRI

Cardiac MRI is the current gold standard for the assessment of cardiac structure, function, and volume.<sup>13</sup> MRI provides excellent anatomical assessment due to its high spatial resolution as well as soft tissue contrast. This allows detailed tissue characterization in pathological processes, especially myocardial fibrosis. MRI is routinely used to assess the myocardium, but it is also capable of assessing smaller structures including the coronary arteries.

## Magnetic Resonance Angiography

Magnetic resonance angiography (MRA) of the coronary arteries can be performed with or without the use of intravascular contrast. The most commonly used contrast agents for coronary MRA are chelated gadolinium-based contrast media which shorten the blood pool T1 relaxation times and enhance the coronary artery lumen.<sup>14</sup> Contrast-enhanced

View this article online at [wileyonlinelibrary.com](http://wileyonlinelibrary.com). DOI: 10.1002/jmri.28554

Received May 10, 2022, Accepted for publication Nov 23, 2022.

\*Address reprint requests to: M.C.W., Chancellor's Building, 49 Little France Crescent, Edinburgh EH16SUF, UK. E-mail: [michelle.williams@ed.ac.uk](mailto:michelle.williams@ed.ac.uk)

From the <sup>1</sup>BHF Centre for Cardiovascular Science, University of Edinburgh, Edinburgh, UK; and <sup>2</sup>Edinburgh Imaging Facility QMRI, University of Edinburgh, Edinburgh, UK

**TABLE 1. Key Research Studies Using Hybrid PET-MRI in Coronary Artery Disease**

Author	Date	PET Tracer	Target for PET Tracer	Key Findings
<i>Atherosclerotic plaque uptake</i>				
Robson et al <sup>4</sup>	2017	<sup>18</sup> F-NaF <sup>18</sup> F-FDG	Microcalcification Inflammation	<sup>18</sup> F-NaF and <sup>18</sup> F-FDG uptake localized to individual coronary artery lesions <sup>18</sup> F-NaF uptake in a culprit plaque post-myocardial infarction
Andrews et al <sup>5</sup>	2021	<sup>18</sup> F-NaF	Microcalcification	PET-MRI uptake was comparable to PET-CT in patients with recent myocardial infarctions <sup>18</sup> F-NaF uptake identified in culprit plaques
<i>Myocardial uptake</i>				
Rischpler et al <sup>6</sup>	2016	<sup>18</sup> F-FDG	Inflammation	PET-MRI uptake is inversely associated with poorer functional outcome, independent of infarction size
Rischpler et al <sup>7</sup>	2015	<sup>18</sup> F-FDG	Inflammation	PET-MRI uptake agrees with MRI LGE for the assessment of viability following revascularization
Vitadello et al <sup>8</sup>	2020	<sup>18</sup> F-FDG	Inflammation	PET-MRI improved diagnostic accuracy for predicting wall motion recovery after revascularization of CTO when compared to PET or MRI alone
Marchesseau et al <sup>9</sup>	2018	<sup>18</sup> F-NaF	Microcalcification	PET-MRI uptake in infarcted myocardium
Notohamiprodjo et al <sup>10</sup>	2021	<sup>68</sup> GA-FAPI	Fibroblasts	PET-MRI uptake in infarcted myocardium
Kunze et al <sup>11</sup>	2018	<sup>13</sup> NH <sub>3</sub>	Myocardial perfusion	Good agreement in MBF between PET and MRI but thresholds for ischemic classification are not directly interchangeable
Kero et al <sup>12</sup>	2021	<sup>15</sup> O-Water	Myocardial perfusion	PET-MRI MBF correlates with MRI MBF, but with only moderate agreement

CTO = chronic total occlusion; LGE = late gadolinium enhancement; <sup>18</sup>F-Na = <sup>18</sup>F-sodium fluoride; CT = computed tomography; <sup>18</sup>F-FDG = <sup>18</sup>F-fluorodeoxyglucose; MBF = myocardial blood flow; MRI = magnetic resonance imaging; PET = positron emission tomography.

coronary MRA has good diagnostic accuracy for the identification of coronary stenoses compared to invasive coronary angiography, particularly in the proximal vessels.<sup>15</sup> Alternative contrast agents for coronary MRA include ultrasmall superparamagnetic iron oxide (USPIO), long-circulating nanoparticles which cause local magnetic field inhomogeneities which increase the R2\* relaxation times (Fig. 2). USPIO are also taken up by inflammatory cells, including macrophages, and identify areas of active tissue inflammation in the myocardium of patients with acute myocardial infarction,<sup>16</sup>

the aortic wall of patients with abdominal aortic aneurysms<sup>17</sup> and the carotid<sup>18</sup> or femoral atherosclerotic plaques<sup>19</sup> of patients with cerebrovascular or peripheral arterial disease. Further research is required to assess whether USPIO could also identify active inflammation in coronary atheroma.

Non-contrast MRA sequences have been developed with good diagnostic accuracy, which can rule out the presence of significant coronary artery stenosis when compared to invasive coronary angiography. A recent meta-analysis showed that non-contrast coronary MRA had a pooled per patient sensitivity and

specificity of 90.3% (95% CI 85.6%–95.1%) and 77.9% (95% CI 69.5%–86.3%) respectively for the detection of >50% coronary artery stenosis when compared to invasive coronary angiography.<sup>20</sup> The major advantages of non-contrast MRA are the lack of ionizing radiation or gadolinium-based contrast media, which is why it is often used in pediatric age groups.

Recent technological advances have further improved the diagnostic accuracy of coronary MRA. The lengthy scan acquisition times have been reduced with advances such as the use of compressed sensing whole heart coronary MRA, which shortens scan times without loss of diagnostic image quality.<sup>21</sup> Spatial resolution and signal-to-noise ratio have been improved with novel technology such as super-resolution imaging and deep learning reconstruction.<sup>22</sup> The issue of respiratory motion blurring had been previously addressed through breath holding techniques, although this limited the amount of data that could be acquired and thus reduced the spatial resolution. Self-navigated techniques which measure the displacement of the heart directly have increased spatial resolution as well as scanner efficiency.<sup>23</sup>

MRI can identify features of high-risk atherosclerotic plaques in the carotid and coronary arteries, such as positive remodeling, large lipid rich necrotic cores, thin fibrous caps, intraplaque hemorrhage, intraluminal thrombus and angiogenesis (Fig. 1).<sup>24–26</sup> Through the use of non-contrast T1 weighted imaging, high-intensity coronary plaque has been suggested to represent intracoronary thrombus or intraplaque hemorrhage, and potentially the vulnerable plaque.<sup>27</sup> These high-intensity plaques are significantly associated with coronary events and may serve as a predictor of future cardiac events.<sup>28</sup>

The small caliber and complex motion of the coronary arteries can lead to image degradation on MRI and reduces

the specificity and sensitivity of coronary artery assessment compared to computed tomography (CT) coronary angiography. Due to their low proton density, calcification and intracoronary stents cause signal drop-out and susceptibility artifacts on MRI, which can affect assessment of the coronary arteries.<sup>22</sup> However, the lack of ionizing radiation makes MRI an attractively imaging modality, especially for use in younger patients or where sequential scanning is needed. Nevertheless, the higher cost, longer acquisition times, and patient contraindications have meant that MRI has lagged behind CT when it comes to coronary artery assessment.<sup>13</sup>

### Positron Emission Tomography

PET uses radionuclides that emit positrons to generate images of metabolic activity. These positron emitters are produced artificially by a cyclotron or generator and are used to label specific biological compounds. The most commonly used PET radiotracer is <sup>18</sup>F-fluorodeoxyglucose (FDG), an analogue of glucose which is widely used in cancer imaging. However, a variety of other established and novel radiotracers have shown promise in the assessment of CAD (Fig. 1). PET radiotracers are injected intravenously and given time to circulate throughout the body to allow uptake by the target. The PET scanner detects the photons which are released in opposite directions after a positron from the radiotracer encounters an electron and an annihilation event occurs.<sup>29</sup> PET is highly specific for targeting metabolic pathways, cell surface markers, and receptors. When it is combined with anatomical imaging such as CT or MRI, anatomical localization of specific biological processes can be identified. Thus, PET-MRI has the potential to identify early subclinical CAD,

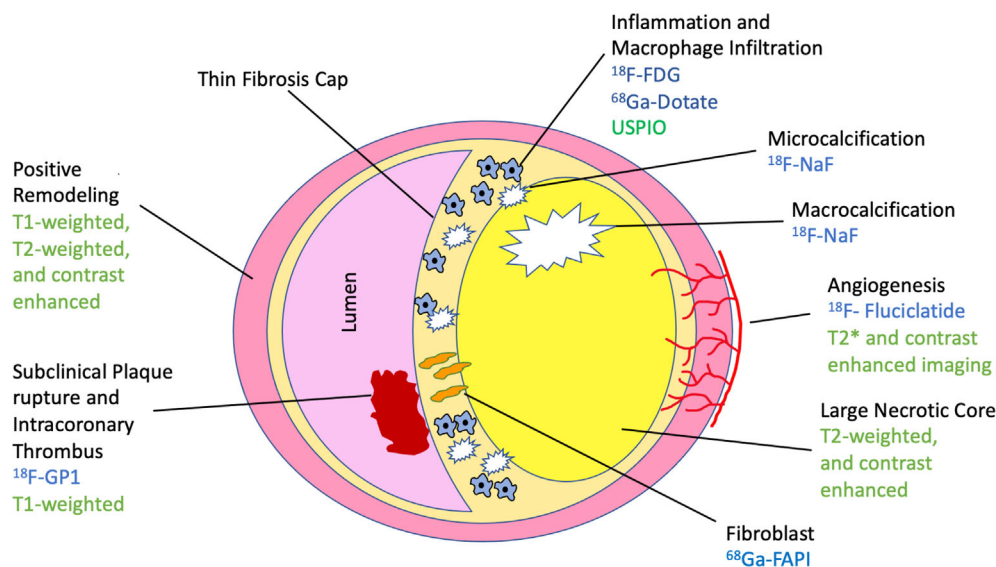


**FIGURE 1:** PET and MRI imaging in coronary artery disease. Illustration demonstrating PET (blue) and MR (green) imaging targets in high-risk atherosclerotic plaque. PET = positron emission tomography; MR = magnetic resonance; <sup>18</sup>F-FDG = <sup>18</sup>F-fluorodeoxyglucose; <sup>18</sup>F-Na = <sup>18</sup>F-sodium fluoride; FAPI = fibroblast activation protein inhibitors; USPIOs = ultrasmall superparamagnetic iron oxide.

to discern active vs. stable disease, and to monitor responses to therapy or disease progression.

### Hybrid PET-MRI

PET is usually combined with CT (PET-CT) due to the difficulty of developing photomultiplier detectors capable of functioning within strong magnetic fields. However, in 2010, the first hybrid PET-MRI scanner was developed.<sup>30</sup> Compared to PET-CT, PET-MRI has several advantages including improved tissue characterization and reduced radiation dose.

Prior to the development of the PET-MRI scanner, it was possible to combine PET and MRI images obtained from separate scanners using image registration techniques. This is a complex process that requires a computation algorithm provided by imaging software. As well as the complexity of this process, there may be misalignment due to patient movement or involuntary motion of organs between the two sequential scans which reduce the spatial registration. In contrast, the hybrid PET-MRI system acquires both MRI and PET images at the same time which enables near perfect co-registration, and acquisition times are also reduced. Near perfect co-registration is important for myocardial perfusion PET-MR imaging and for the imaging of small structures, such as the coronary arteries. The limitations of the hybrid PET-MRI system are its higher cost and limited availability.<sup>4</sup> MRI sequences may also need to be adjusted for use in the PET-MRI scanner.

For cardiac imaging, PET-MRI can combine anatomical, functional, and metabolic assessment in one investigation. Given the significant reduction in radiation dose compared to PET-CT, PET-MRI lends itself to longitudinal imaging studies where disease progression or therapeutic response can be assessed.

### PET-MRI Coronary Artery Imaging

Several radiotracers have been used to assess the coronary arteries in research studies, including established radiotracers such as <sup>18</sup>F-FDG, repurposed radiotracers such as <sup>18</sup>F-sodium fluoride (<sup>18</sup>F-NaF), and novel radiotracers such as <sup>18</sup>F-GP1 (a derivative of elarofiban, an antagonist to the platelet glycoprotein IIb/IIIa receptor). These each target different biological processes and can therefore inform on different aspects of CAD.

#### <sup>18</sup>F-Fluorodeoxyglucose

Inflammation plays a central role in atherosclerosis and is thought to be a key precipitant in acute plaque rupture. Inflammatory cells, such as macrophages, are thought to infiltrate and weaken the fibrous cap of atherosclerotic plaques, predisposing the plaque to rupture.<sup>31</sup> <sup>18</sup>F-FDG is a glucose analogue which is taken up by cells which have high glucose utilization and hence high metabolic demand. Principally, it has been used in patients with suspected or established cancer

but more recently it has been studied in those with atherosclerosis. Most vascular studies to date use PET-CT in large arteries such as the carotid arteries, femoral arteries, or aorta. Increased <sup>18</sup>F-FDG uptake is associated with the presence of cardiovascular risk factors<sup>32</sup> and morphological high-risk plaque features.<sup>33</sup> Reductions in large vessel <sup>18</sup>F-FDG uptake have been demonstrated in response to statin therapy.<sup>34</sup> Rudd et al identified <sup>18</sup>F-FDG uptake in culprit carotid atherosclerotic plaques when compared to non-culprit plaques,<sup>35</sup> although more recent studies demonstrated more overlap in <sup>18</sup>F-FDG uptake between such lesions.<sup>36</sup> Similarly in the coronary arteries, Joshi et al found no difference between <sup>18</sup>F-FDG uptake in culprit and non-culprit vessels on PET-CT.<sup>37</sup> Robson et al were the first to study coronary <sup>18</sup>F-FDG uptake using PET-MRI in 23 patients. This feasibility study demonstrated that elevated <sup>18</sup>F-FDG uptake could be localized to individual coronary lesions and identified a culprit plaque post-myocardial infarction in the left anterior descending coronary artery.<sup>38</sup>

The main weakness of coronary artery <sup>18</sup>F-FDG imaging is the impact of the physiological uptake of <sup>18</sup>F-FDG by the myocardium. Such uptake causes substantial overspill of signal and obscures the coronary arteries. Reduced myocardial <sup>18</sup>F-FDG uptake can be achieved by asking patients to fast for over 12 hours prior to the scan. However, this does not cause complete suppression of uptake and often leaves patchy uptake of the tracer. Indeed, in those undergoing PET-MRI, 75% of patients have some persistent physiological myocardial <sup>18</sup>F-FDG uptake which limited the assessment of coronary activity in one or more coronary territories.<sup>38</sup> More consistent methods of reducing physiological myocardial uptake would be required to make this tracer useful for routine coronary imaging.

#### <sup>18</sup>F-Sodium Fluoride

Large macroscopic calcification is a well-known feature of human atherosclerosis and can be easily detected by CT. However, imaging at this late stage often means that the processes preceding this have resolved and active disease may be absent. The earlier stages of developing microcalcification are a biologically more interesting stage of the disease, being associated with plaque inflammation, ongoing disease activity, and an increased risk of rupture.<sup>39,40</sup> <sup>18</sup>F-Sodium fluoride (<sup>18</sup>F-NaF) is an established PET tracer which was initially used to identify bone metastases, as its uptake is increased in areas of new bone formation or high bone turnover.<sup>41</sup> Following intravenous injection, it diffuses through the capillary network and when it encounters exposed regions of hydroxyapatite crystals, it exchanges a hydroxyl group to form fluoroapatite. The specific binding of <sup>18</sup>F-NaF to hydroxyapatite has been validated in ex vivo studies.<sup>42</sup> Hydroxyapatite is a key component of vascular calcification and has a larger surface area in areas of microcalcification compared to



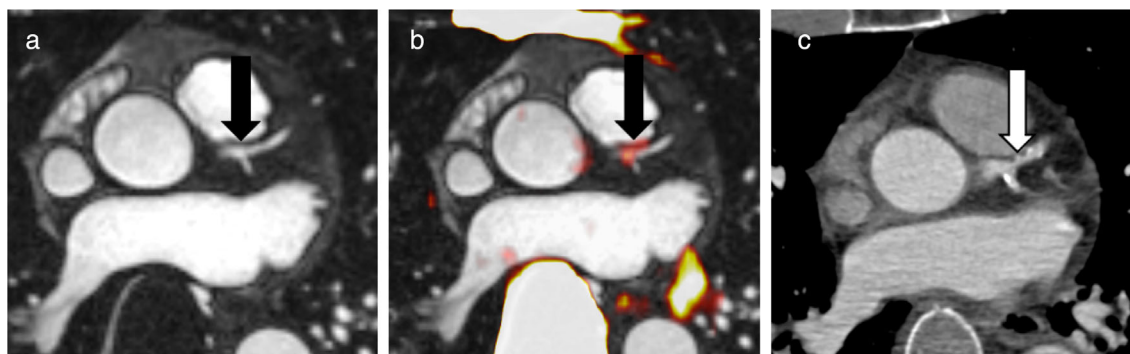


**FIGURE 2:** PET-MRI of the coronary arteries with  $^{18}\text{F}$ -sodium fluoride. USPIO contrast-enhanced MRI (a),  $^{18}\text{F}$ -NaF PET-MRI (b) and CT coronary angiography (c) images from a 61-year-old male with a recent anterior ST elevation myocardial infarction and stenting of the mid left anterior descending coronary artery. PET-MRI shows  $^{18}\text{F}$ -NAF uptake (black arrow) in the distal left mainstem and proximal LAD where there is non-obstructive plaque on MRI (black arrow) and non-calcified plaque on CT (white arrow).

macroscopic calcium deposits.<sup>43</sup> As a result, increased  $^{18}\text{F}$ -NaF uptake is observed in regions of developing microcalcification and has been identified in culprit and high-risk coronary lesions assessed with PET-CT.<sup>37</sup>

Robson et al<sup>38</sup> were the first to demonstrate PET-MRI of the coronary arteries with  $^{18}\text{F}$ -NaF in a feasibility study. They recruited 23 patients with CAD or cardiovascular risk factors and identified focal  $^{18}\text{F}$ -NaF uptake in four patients with CAD, including a culprit lesion in the left anterior descending coronary artery. Andrews et al performed both  $^{18}\text{F}$ -NaF PET-MRI and PET-CT in patients with recent myocardial infarction or aortic stenosis.<sup>5</sup> They found that  $^{18}\text{F}$ -NaF uptake was common in culprit plaques and that the pattern of uptake was similar between PET-CT and PET-MRI in non-stented coronary arteries. They showed that the maximum standard uptake values ( $\text{SUV}_{\text{max}}$ ) were higher from PET-CT than PET-MRI, but maximum target-to-background ratio ( $\text{TBR}_{\text{max}}$ ) were comparable. Further research is required to assess the clinical utility of the additional information that can be obtained from  $^{18}\text{F}$ -NaF PET-MRI of the coronary arteries (Fig. 2). Indeed a preliminary study in carotid arteries in patients undergoing carotid endarterectomy showed complementary information from MRI plaque analysis and  $^{18}\text{F}$ -NaF uptake.<sup>24</sup>

### $^{18}\text{F}$ -GP1

$^{18}\text{F}$ -GP1 is a derivative of elarofiban which is a highly selective and specific inhibitor activated glycoprotein IIb/IIIa receptors on platelets. Given its specificity for activated platelets, it is a highly selective radiotracer for identifying fresh arterial and venous thromboses.<sup>44,45</sup> A recent PET-CT study of bio-prosthetic aortic valves showed that  $^{18}\text{F}$ -GP1 bound selectively to activated platelet glycoprotein IIb/IIIa receptors and thrombus, and regressed with antithrombotic therapy.<sup>46</sup> Early case reports have shown the potential for  $^{18}\text{F}$ -GP1 to identify coronary and cardiac thrombus formation in the presence of intracoronary stents.<sup>47</sup> This technique has the potential to

differentiate between a type 1 and type 2 myocardial infarction as well as aid in diagnosis of patients presenting with myocardial infarctions who have normal coronary arteries on invasive coronary angiography.  $^{18}\text{F}$ -GP1 has the potential to assess thrombus formation in other vascular territories and ongoing studies will assess its application in cardiac and coronary structures (iThrombus, NCT03943966).

## PET-MRI and Myocardial Imaging in Coronary Artery Disease

### Myocardial Perfusion

Cardiac MRI and PET are both established techniques for the assessment of myocardial perfusion.<sup>48,49</sup>  $^{15}\text{O}$ -Water PET-CT myocardial perfusion imaging has superior image quality, spatial resolution, and diagnostic accuracy compared to single photon emission CT.<sup>48</sup> Other radiotracers have been used for PET-CT myocardial perfusion imaging including  $^{13}\text{N}$ -ammonia,  $^{82}\text{Rb}$  rubidium, and  $^{18}\text{F}$ -Flurpiridaz. However, availability of PET-CT scanners and radiotracers currently limits the more widespread use of PET myocardial perfusion imaging in clinical practice.

PET-MRI can also be used to assess myocardial perfusion. Kunze et al explored the potential for  $^{13}\text{N}$ -ammonia PET-MRI for myocardial perfusion imaging.<sup>11</sup> They found overall good agreement between PET and MRI for the assessment of absolute myocardial perfusion flow. However, they suggest that the absolute thresholds for ischemic classification by PET and dynamic contrast-enhanced MRI may not be directly interchangeable as MRI underestimated coronary flow reserve because of an overestimation of resting perfusion. In a small study of 15 patients, Kero et al assessed  $^{15}\text{O}$ -water PET-MRI myocardial blood flow and found a good correlation and moderate agreement with simultaneous dynamic contrast-enhanced MRI assessments of myocardial blood flow.<sup>12</sup> Further work is required to assess how PET-MRI myocardial perfusion can be integrated with the other

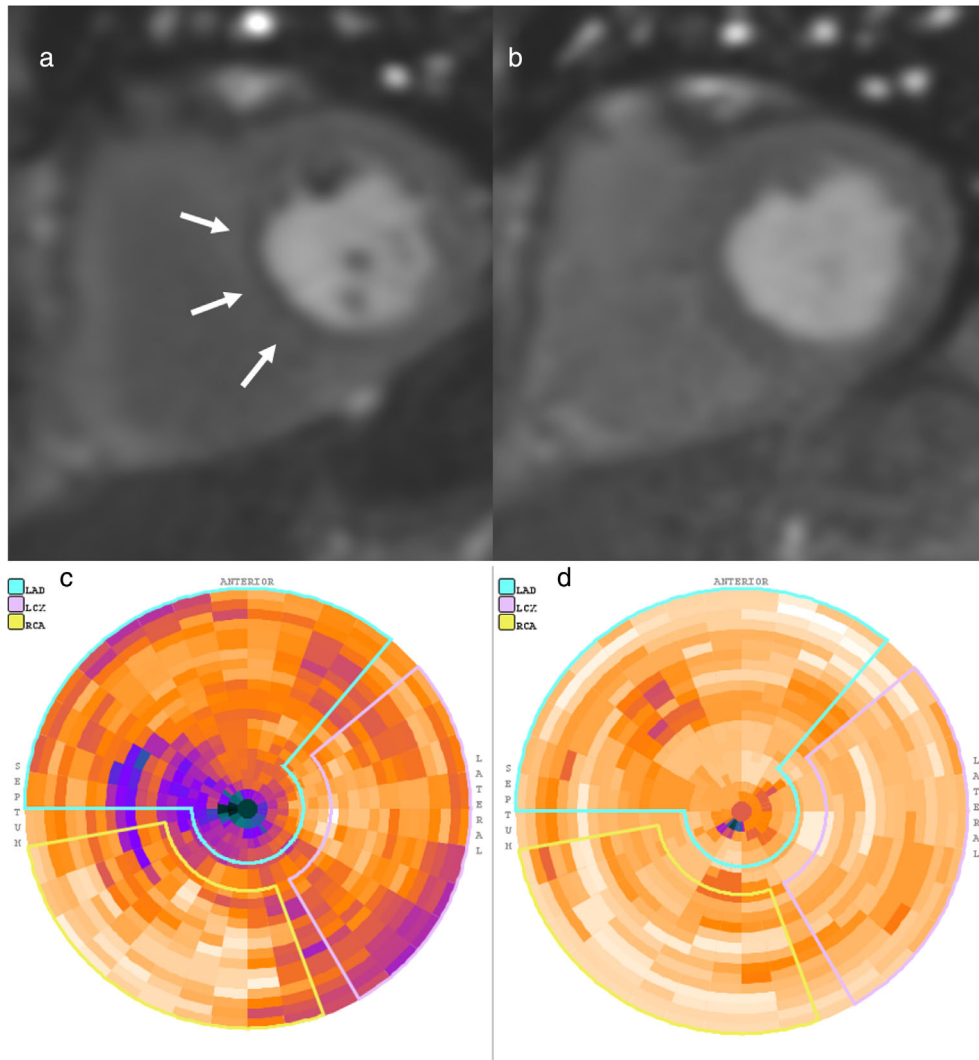


**FIGURE 3:** PET-MRI myocardial perfusion imaging with  $^{15}\text{O}$ -oxygen-water. Images from rest (b, d) and adenosine stress (a, c) show a reversible inferior and inferoseptal subendocardial perfusion defect on dynamic contrast-enhanced MRI (a, b). Reduced myocardial perfusion was identified on quantitative analysis of adenosine stress  $^{15}\text{O}$ -oxygen-water PET (c, purple/blue) which returned to normal on rest imaging (d, yellow/orange). Courtesy of Dr Sohaib Nazir.

structural and functional information available from MRI imaging (Fig. 3).

### Myocardial Viability and Functional Recovery

Cardiac MRI is widely used in clinical practice to assess myocardial viability.<sup>50</sup> PET with  $^{18}\text{F}$ -FDG can also be used to assess myocardial viability. Rischpler et al studied whether it would be feasible to combine PET and late-gadolinium MRI information obtained using a hybrid PET-MRI scanner. They found that the simultaneous assessment of late gadolinium enhancement on MRI and  $^{18}\text{F}$ -FDG uptake was feasible and showed substantial inter-method agreement (kappa 0.65) for predicting myocardial viability following revascularization. They noted that the small discrepancies between  $^{18}\text{F}$ -FDG PET and MRI late-gadolinium enhancement were due to the superior predictor of functional recovery provided by  $^{18}\text{F}$ -FDG.<sup>7</sup> A study of  $^{18}\text{F}$ -FDG PET-MRI in patients with

coronary artery chronic total occlusion showed only slight inter-method agreement in viability assessment between the two modalities (kappa 0.1). However, it did show the best predictor of wall motion recovery was combined  $^{18}\text{F}$ -FDG PET-MRI (area under the curve [AUC] 0.72), compared to late gadolinium MRI (AUC 0.66) or  $^{18}\text{F}$ -FDG PET alone (AUC 0.58).<sup>8</sup>

There has been interest in the use of hybrid PET-MRI imaging for predicting functional outcome following acute myocardial infarction. Rischpler et al recruited 49 patients following ST-segment elevation myocardial infarction and performed  $^{18}\text{F}$ -FDG PET-MRI imaging 5 days after percutaneous coronary intervention and cardiac MRI 6 months later.<sup>6</sup> They found that the intensity of early  $^{18}\text{F}$ -FDG signal was inversely associated with MRI measures of left ventricular global and regional functional outcome, independent of the size of the infarction. This highlights a potential prognostic

role for post-infarct  $^{18}\text{F}$ -FDG PET-MRI, but further research is required to validate this in a larger cohort.

Radiotracers used for bone scintigraphy, such as the technetium-99m labeled phosphate analogues, are known to accumulate in sites of infarction, such as the myocardium.<sup>51</sup>  $^{18}\text{F}$ -NaF has also been used to assess myocardial infarction with PET-MRI. In a small study of 10 patients with myocardial infarction, Marchesseu et al showed that myocardial  $^{18}\text{F}$ -NaF uptake could be detected in the territory supplied by the infarct-related artery using both PET-CT and PET-MRI. They found increased  $^{18}\text{F}$ -NaF uptake in the infarcted myocardium on both PET-CT and PET-MR compared to the remote myocardium.<sup>9</sup>

Activated fibroblasts play a key role in the development of fibrosis and remodeling following myocardial infarction. Fibroblast activation protein is a specific marker of activated fibroblasts. Using  $^{68}\text{Ga}$  or  $^{18}\text{F}$  labeled fibroblast activation protein inhibitors (FAPI), fibrosis can be directly visualized using PET. FAPI PET tracers have shown great promise in the assessment of a variety of cancers<sup>52</sup> but fibrosis also plays an important role in cardiovascular diseases (Fig. 4). High left ventricular  $^{68}\text{Ga}$ -FAPI uptake on PET-CT correlated to the presence of cardiovascular risk factors in a meta-analysis of 229 patients with metastatic cancer.<sup>53</sup> The first published case of  $^{68}\text{Ga}$ -FAPI in human myocardial infarction observed intense uptake on PET-MRI 6 days following myocardial infarction.<sup>10</sup> Ongoing studies will assess the clinical utility of FAPI PET-MRI in myocardial infarction (The FAPI-Fibrosis study, NCT05356923). There has been a recent retrospective study of  $^{68}\text{Ga}$ -FAPI uptake in segments of aortas and iliac arteries using PET-CT. Elevated uptake occurred in non-calcified arterial segments when compared to advanced chronic lesions and increased arterial uptake in patients with more cardiovascular risk factors. Immunohistochemical labeling of carotid plaques also found prominent FAPI expression in thin fibrous caps compared to moderate

expression in thick caps.<sup>54</sup> As yet, no studies have assessed coronary  $^{68}\text{Ga}$ -FAPI uptake although there is potential for this radiotracer to assess atherosclerotic fibroblast activity in other vascular territories.

### Intra-Cardiac Thrombus

The development of left ventricular thrombus following myocardial infarction is also a potential target for PET-MRI imaging.  $^{18}\text{F}$ -GP1 has been identified in left ventricle thrombus, intramyocardial microvascular obstruction, and left atrial appendage thrombus.<sup>55</sup> The formation of a left ventricular cavity thrombus following myocardial infarction often passes undetected and poses a significant risk of stroke. We currently have little evidence on the natural history of this condition with no randomized controlled trials having yet evaluated the efficacy of anticoagulation or its optimal duration of therapy.<sup>56</sup> Ongoing research (MyoThrombus, NCT04829825) is exploring the detection of subclinical left ventricular thrombus following anterior ST-elevation myocardial infarction as well monitoring response to anticoagulant therapy. This technique also has potential to detection microvascular obstruction and intra-myocardial hemorrhage following myocardial infarction, which can be seen as  $^{18}\text{F}$ -GP1 uptake within infarcted myocardium itself. This could provide further insight into cardiac remodeling and prognostic indicators following myocardial infarction (Figs. 5 and 6).

### PET-MRI Challenges and Future Directions

Important technical challenges for PET-MRI include the small size of the coronary arteries and coronary plaques, cardiac and respiratory motion, and requirements of attenuation correction. Other limitations include long acquisition times, overall cost, and availability of PET-MRI scanners. PET involves the use of ionizing radiation, which must be justified with indications where the PET component of the scan provides information over and above the MRI alone.

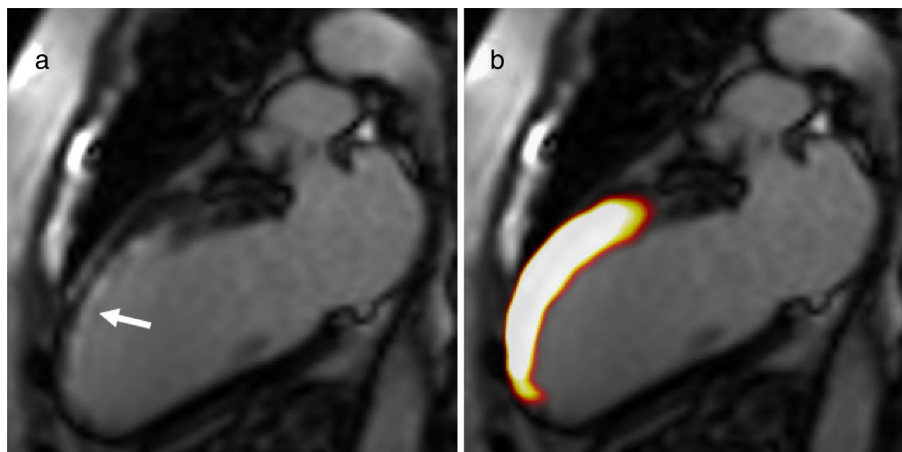
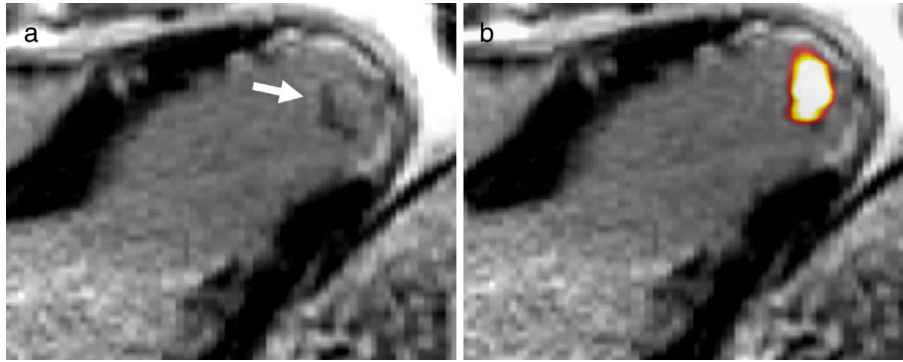
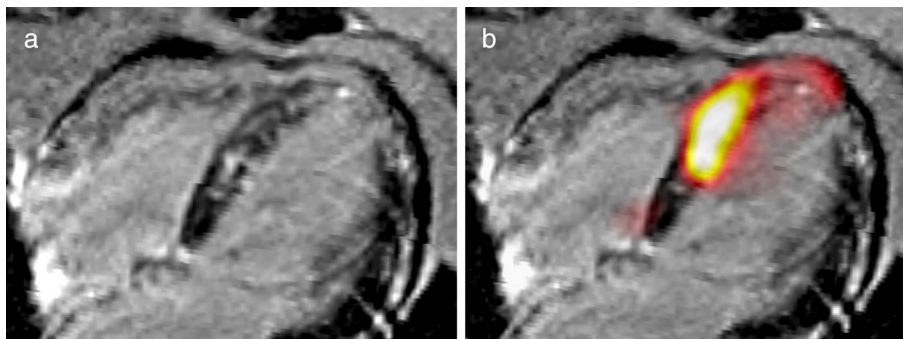


FIGURE 4: PET-MRI imaging of fibroblast activity. MRI (a) and  $^{68}\text{Ga}$ -FAPI (b) PET-MRI images from a 75-year-old with a recent anterior ST elevation myocardial infarction.  $^{68}\text{Ga}$ -FAPI uptake within myocardium corresponds to area of late gadolinium enhancement seen on MRI (white arrow). Images courtesy of Dr Anna Barton.





**FIGURE 5:** PET-MRI of intra-cardiac thrombus. MRI (a) and  $^{18}\text{F}$ -GP1 PET-MRI (b) from 62-year-old male with recent out of hospital cardiac arrest secondary to an anterior ST elevation myocardial infarction.  $^{18}\text{F}$ -GP1 PET-MRI shows uptake (maximum tissue background ratio 2.5) corresponding to apical left ventricular thrombus (white arrow) seen on MRI adjacent to the apical myocardial late gadolinium enhancement. Images courtesy of Dr Evangelos Tzolos.



**FIGURE 6:** PET-MRI of microvascular obstruction and hemorrhage. MRI (a) and  $^{18}\text{F}$ -GP1 PET-MRI (b) images of a 69-year-old lady presenting with an anterior ST elevation myocardial infarction secondary to stent thrombosis in the left anterior descending artery. High  $^{18}\text{F}$ -GP1 uptake within the septal left ventricle myocardium is associated with late gadolinium uptake representing microvascular obstruction/hemorrhage. Images courtesy of Dr Evangelos Tzolos.

The radiation dose of PET-MRI will be lower than PET-CT and this may enable more wider use of PET imaging and the potential for follow-up imaging. Neither of these techniques are currently widely used for clinical coronary artery imaging, but research in this field is rapidly advancing.

PET-MRI is challenging in small structures, such as the coronary arteries. MRI can overestimate stenosis severity and PET imaging can underestimate lesion activity and hamper accurate quantification. The optimum method to assess coronary PET radiotracer uptake is currently unknown. Visual assessment of a lesion can provide qualitative data on PET uptake, but this relies on correct window settings on appropriate software. Quantitative analysis is therefore more usually performed, where the user delineates a region of interest to assess the standardized uptake value (SUV) and compares this with the background SUV activity obtained from a homogeneous vascular structure, such as the right atrium. This is termed the tissue-to-background ratio (TBR). This process is labor intensive and only assesses the activity in individual lesions. A new technique has therefore been developed to assess  $^{18}\text{F}$ -NaF uptake across the coronary tree, called the coronary microcalcification activity (CMA). This automated technique assesses  $^{18}\text{F}$ -NaF uptake across the entire coronary

vasculature and has close agreement to CT markers of plaque vulnerability.<sup>57</sup>

PET-MRI attenuation correction remains a challenge given that, unlike with CT, tissue density cannot be measured directly. The image artifacts at the heart-lung boundary pose a particular issue. Robson et al described the use of a free-breathing, golden-angle radial MRI acquisition for PET attenuation correction as well as increasing the number of iterations for PET reconstruction.<sup>38</sup> This approach improved image quality, reduced extra-cardiac artifacts, and enhanced the SUV and TBR of coronary lesions. Most commercially available PET/MR systems use an atlas or segmental-based methods for MR/PET attenuation. Segmental errors, incorrectly assigned tissue models, and artifacts due to bone or metal implants can all lead to inconsistencies in the attenuation correction maps and impact the diagnostic quality of the resulting PET images.<sup>58</sup> There have been some promising recent developments in specific attenuation correction sequences such as the CAIPIRINHA (controlled aliasing in parallel imaging results in higher acceleration) accelerated T1-weighted 3D-VIBE sequence. This has produced MR images with higher resolution compared to standard VIBE DIXON sequences, whilst maintaining comparable scan

times of 19 seconds per bed position.<sup>59</sup> New techniques aim to use machine learning techniques to improve attenuation correction sequences.<sup>60</sup> PET reconstructions have also become more robust, including the introduction of time-of-flight (TOF) reconstructions, which are widely used in PET/CT. TOF technology can help reduce scan time, reduce injected radiotracer dose, and improve signal-to-noise ratio and lesion detectability, particularly in patients with higher body mass index.<sup>61</sup>

Motion correction is another important cause of image degradation in PET imaging. Techniques used in CT imaging are not feasible as gating images would cause desirable tracer counts to be missed and breath holding is not possible as PET images are acquired over minutes. A recent technique to address this challenge uses direct anatomical data from the MRI to track patient motion. This can be used to create 3D motion fields for PET motion correction. When compared to non-motion corrected 18-FDG PET/MR cardiac imaging, these motion corrected images showed less blurring, improved alignment of tracer activity and myocardial anatomy, and greater contrast to noise ratio.<sup>62</sup> This motion correction method has also been shown to improve fully quantitative cardiac dynamic PET studies.<sup>63</sup>

Coronary PET-MRI is limited by the presence of intracoronary stents. This is due to the magnetic field inhomogeneities causing signal loss on MRI images, which then also impact on the attenuation correction of the PET data.<sup>5</sup> This results in severe artifacts caused by drop out of PET signal at the site of stent implantation. The use of novel MR gap-filling algorithms has shown promise in overcoming this limitation.<sup>64</sup>

The development of new methods of patient preparation for <sup>18</sup>F-FDG imaging may improve signal-to-noise ratios for both coronary and myocardial imaging. In addition, the development of new specific novel radiotracers, particularly those with no physiological myocardial uptake, holds promise for the future. For example, in PET-CT studies, <sup>68</sup>Ga-DOTATATE, a PET ligand with binding affinity for somatostatin receptor-2 on activated macrophages, is a marker of coronary atherosclerotic inflammation<sup>65</sup> and infarcted myocardium.<sup>66</sup> <sup>18</sup>F-Fluciclatide, an arginine-glycine-aspartate (RGD) tripeptide radiotracer that binds to the transmembrane cell surface receptor  $\alpha_v\beta_3$  integrin on upregulated macrophages and myofibroblasts, is a marker of recent but not prior myocardial infarction with PET-CT.<sup>67</sup> Further exploration of such radiotracers with PET-MRI may lead to an improved understanding of CAD in the future.

## Conclusion

PET-MR has the potential to be a valuable modality for the assessment of CAD. It combines information on disease activity from PET with the excellent anatomical detail and tissue

characterization provided by MRI. It has shown the ability to identify features of high-risk coronary atherosclerotic plaque such as inflammation, microcalcification, and thrombosis. In addition, it has shown encouraging results in the assessment of myocardial viability, functional recovery, and perfusion imaging. This non-invasive and low radiation modality presents a promising alternative to current imaging modalities used in coronary artery assessment. Future research will be required to assess how the combination of information available from PET-MRI can be used in clinical practice.

## Acknowledgments

BW (FS/CRTF/21/24129), MRD (FS/14/78/31020), DEN (CH/09/002, RG/16/10/32375, RE/18/5/34216), and MCW (FS/ICRF/20/26002) are supported by the British Heart Foundation. MCW is supported by The Chief Scientist Office of the Scottish Government Health (PCL/17/04) and The Academy of Medical Sciences (SGL016\1059). EVB is supported by SINAPSE ([www.sinapse.ac.uk](http://www.sinapse.ac.uk)). Images courtesy of Dr Sohaib Nazir, Dr Anna Barton, and Dr Evangelos Tzolos.

## Conflict of Interest

Dr Williams has given lectures at meetings sponsored by Canon Medical Systems and Siemens Healthineers.

## References

1. Townsend N, Wilson L, Bhatnagar P, Wickramasinghe K, Rayner M, Nichols M. Cardiovascular disease in Europe: Epidemiological update 2016. *Eur Heart J* 2016;37(42):3232-3245.
2. Bentzon JF, Otsuka F, Virmani R, Falk E. Mechanisms of plaque formation and rupture. *Circ Res* 2014;114(12):1852-1866.
3. Nensa F, Bamberg F, Rischpler C, et al. Hybrid cardiac imaging using PET/MRI: A joint position statement by the European Society of Cardiovascular Radiology (ESCR) and the European Association of Nuclear Medicine (EANM). *Eur Radiol* 2018;28(10):4086-4101.
4. Robson PM, Dey D, Newby DE, et al. MR/PET imaging of the cardiovascular system. *JACC Cardiovasc Imaging* 2017;10(10 Pt A):1165-1179.
5. Andrews JPM, MacNaught G, Moss AJ, et al. Cardiovascular 18F-fluoride positron emission tomography-magnetic resonance imaging: A comparison study. *J Nucl Cardiol* 2021;28(5):1-12.
6. Rischpler C, Dirschinger RJ, Nekolla SG, et al. Prospective evaluation of 18F-fluorodeoxyglucose uptake in postischemic myocardium by simultaneous positron emission tomography/magnetic resonance imaging as a prognostic marker of functional outcome. *Circ Cardiovasc Imaging* 2016;9(4):e004316.
7. Rischpler C, Langwieser N, Souvatzoglou M, et al. PET/MRI early after myocardial infarction: Evaluation of viability with late gadolinium enhancement transmurality vs. 18F-FDG uptake. *Eur Heart J Cardiovasc Imaging* 2015;16(6):661-669.
8. Vitadello T, Kunze KP, Nekolla SG, et al. Hybrid PET/MR imaging for the prediction of left ventricular recovery after percutaneous revascularisation of coronary chronic total occlusions. *Eur J Nucl Med Mol Imaging* 2020;47(13):3074-3083.
9. Marchesseau S, Seneviratna A, Sjöholm AT, et al. Hybrid PET/CT and PET/MRI imaging of vulnerable coronary plaque and myocardial scar

- tissue in acute myocardial infarction. *J Nucl Cardiol* 2018;25(6):2001-2011.
10. Notohamiprodjo S, Nekolla SG, Robu S, et al. Imaging of cardiac fibroblast activation in a patient after acute myocardial infarction using (68)Ga-FAPI-04. *J Nucl Cardiol* 2022;29:2254-2261.
  11. Kunze KP, Nekolla SG, Rischpler C, et al. Myocardial perfusion quantification using simultaneously acquired (13)NH(3)-ammonia PET and dynamic contrast-enhanced MRI in patients at rest and stress. *Magn Reson Med* 2018;80(6):2641-2654.
  12. Kero T, Johansson E, Engström M, et al. Evaluation of quantitative CMR perfusion imaging by comparison with simultaneous (15)O-water-PET. *J Nucl Cardiol* 2021;28(4):1252-1266.
  13. Mangla A, Oliveros E, Williams KA, Kalra DK. Cardiac imaging in the diagnosis of coronary artery disease. *Curr Probl Cardiol* 2017;42(10):316-366.
  14. Dweck MR, Puntmann VO, Vesey AT, Fayad ZA, Nagel E. MR imaging of coronary arteries and plaques. *JACC Cardiovasc Imaging* 2016;9(3):306-316.
  15. Schuetz GM, Zacharopoulou NM, Schlattmann P, Dewey M. Meta-analysis: Noninvasive coronary angiography using computed tomography versus magnetic resonance imaging. *Ann Intern Med* 2010;152(3):167-177.
  16. Alam SR, Shah ASV, Richards J, et al. Ultrasmall superparamagnetic particles of iron oxide in patients with acute myocardial infarction. *Circ Cardiovasc Imaging* 2012;5(5):559-565.
  17. MA3RS Study Investigators. Aortic wall inflammation predicts abdominal aortic aneurysm expansion, rupture, and need for surgical repair. *Circulation* 2017;136(9):787-797.
  18. Sadat U, Howarth SPS, Usman A, Tang TY, Graves MJ, Gillard JH. Sequential imaging of asymptomatic carotid atheroma using ultrasmall superparamagnetic iron oxide-enhanced magnetic resonance imaging: A feasibility study. *J Stroke Cerebrovasc Dis* 2013;22(8):e271-e276.
  19. Zheng KH, Schoormans J, Stiekema LCA, et al. Plaque permeability assessed with DCE-MRI associates with USPIO uptake in patients with peripheral artery disease. *JACC Cardiovasc Imaging* 2019;12(10):2081-2083.
  20. Zahergivar A, Kocher M, Waltz J, et al. The diagnostic value of non-contrast magnetic resonance coronary angiography in the assessment of coronary artery disease: A systematic review and meta-analysis. *Heliyon* 2021;7(3):e06386.
  21. Nakamura M, Kido T, Kido T, et al. Non-contrast compressed sensing whole-heart coronary magnetic resonance angiography at 3T: A comparison with conventional imaging. *Eur J Radiol* 2018;104:43-48.
  22. Kato Y, Ambale-Venkatesh B, Kassai Y, et al. Non-contrast coronary magnetic resonance angiography: Current frontiers and future horizons. *Magn Reson Mater Phys Biol Med* 2020;33(5):591-612.
  23. Piccini D, Monney P, Sierro C, et al. Respiratory self-navigated post-contrast whole-heart coronary MR angiography: Initial experience in patients. *Radiology* 2014;270(2):378-386.
  24. Kaczynski J, Williams M, Forsythe R, et al. Early experience with 18F-fluoride positron emission tomography-magnetic resonance imaging in patients with symptomatic carotid artery stenosis undergoing carotid endarterectomy. *Eur J Vasc Endovasc Surg* 2019;58(6):e845-e846.
  25. Fayad ZA, Fuster V. Characterization of atherosclerotic plaques by magnetic resonance imaging. *Ann N Y Acad Sci* 2000;902:173-186.
  26. Jansen CHP, Perera D, Makowski MR, et al. Detection of intracoronary thrombus by magnetic resonance imaging in patients with acute myocardial infarction. *Circulation* 2011;124(4):416-424.
  27. Tomohiro K, Shoichi K, Nobuhiko K, et al. Characterization of hyperintense plaque with noncontrast T1-weighted cardiac magnetic resonance coronary plaque imaging. *JACC Cardiovasc Imaging* 2009;2(6):720-728.
  28. Noguchi T, Kawasaki T, Tanaka A, et al. High-intensity signals in coronary plaques on noncontrast T1-weighted magnetic resonance imaging as a novel determinant of coronary events. *J Am Coll Cardiol* 2014;63(10):989-999.
  29. Camici PG. Positron emission tomography and myocardial imaging. *Heart* 2000 Apr;83(4):475-480.
  30. Krizsan AK, Lajtos I, Dahlbom M, et al. A promising future: Comparable imaging capability of MRI-compatible silicon photomultiplier and conventional photosensor preclinical PET systems. *J Nucl Med* 2015;56(12):1948-1953.
  31. Joshi NV, Toor I, Shah ASV, et al. Systemic atherosclerotic inflammation following acute myocardial infarction: Myocardial infarction begets myocardial infarction. *J Am Heart Assoc* 2015;4(9):e001956.
  32. Tahara N, Kai H, Yamagishi S, et al. Vascular inflammation evaluated by [18F]-fluorodeoxyglucose positron emission tomography is associated with the metabolic syndrome. *J Am Coll Cardiol* 2007;49(14):1533-1539.
  33. Figueroa AL, Subramanian SS, Cury RC, et al. Distribution of inflammation within carotid atherosclerotic plaques with high-risk morphological features. *Circ Cardiovasc Imaging* 2012;5(1):69-77.
  34. Tahara N, Kai H, Ishibashi M, et al. Simvastatin attenuates plaque inflammation: Evaluation by fluorodeoxyglucose positron emission tomography. *J Am Coll Cardiol* 2006;48(9):1825-1831.
  35. Rudd JHF, Warburton EA, Fryer TD, et al. Imaging atherosclerotic plaque inflammation with [18F]-fluorodeoxyglucose positron emission tomography. *Circulation* 2002;105(23):2708-2711.
  36. Vesey AT, Jenkins WSA, Irkle A, et al. (18)F-fluoride and (18)F-fluorodeoxyglucose positron emission tomography after transient ischemic attack or minor ischemic stroke: Case-control study. *Circ Cardiovasc Imaging* 2017;10(3):e004976.
  37. Joshi NV, Vesey AT, Williams MC, et al. 18F-fluoride positron emission tomography for identification of ruptured and high-risk coronary atherosclerotic plaques: A prospective clinical trial. *Lancet* 2014;383(9918):705-713.
  38. Robson PM, Dweck MR, Trivieri MG, et al. Coronary artery PET/MR imaging: Feasibility, limitations, and solutions. *JACC Cardiovasc Imaging* 2017;10(10, Part A):1103-1112.
  39. Adamson PD, Vesey AT, Joshi NV, Newby DE, Dweck MR. Salt in the wound: 18F-fluoride positron emission tomography for identification of vulnerable coronary plaques. *Cardiovasc Diagn Ther* 2015;5(2):150-155.
  40. Vengrenyuk Y, Carlier S, Xanthos S, et al. A hypothesis for vulnerable plaque rupture due to stress-induced debonding around cellular microcalcifications in thin fibrous caps. *Proc Natl Acad Sci U S A* 2006;103(40):14678-14683.
  41. Czernin J, Satyamurthy N, Schiepers C. Molecular mechanisms of bone 18F-NaF deposition. *J Nucl Med* 2010;51(12):1826-1829.
  42. Moss AJ, Sim AM, Adamson PD, et al. Ex vivo 18F-fluoride uptake and hydroxyapatite deposition in human coronary atherosclerosis. *Sci Rep* 2020;10(1):20172.
  43. Creager MD, Hohlfeld T, Hutcheson JD, et al. 18F-fluoride signal amplification identifies microcalcifications associated with atherosclerotic plaque instability in positron emission tomography/computed tomography images. *Circ Cardiovasc Imaging* 2019;12(1):e007835.
  44. Chae SY, Kwon T-W, Jin S, et al. A phase 1, first-in-human study of 18F-GP1 positron emission tomography for imaging acute arterial thrombosis. *EJNMMI Res* 2019;9(1):3.
  45. Kim C, Lee JS, Han Y, et al. Glycoprotein IIb/IIIa receptor imaging with (18)F-GP1 positron emission tomography for acute venous thromboembolism: An open-label, non-randomized, first-in-human phase 1 study. *J Nucl Med* 2018;60(2):244-249.
  46. Bing R, Deutsch M-A, Sellers SL, et al. 18F-GP1 positron emission tomography and bioprosthetic aortic valve thrombus. *JACC Cardiovasc Imaging* 2022;15:1107-1120.
  47. Tzolos E, Bing R, Newby DE, Dweck MR. Categorising myocardial infarction with advanced cardiovascular imaging. *Lancet* 2021;398(10299):e9.

48. Danad I, Raijmakers PG, Driessen RS, et al. Comparison of coronary CT angiography, SPECT, PET, and hybrid imaging for diagnosis of ischemic heart disease determined by fractional flow reserve. *JAMA Cardiol* 2017;2(10):1100-1107.
49. Nagel E, Greenwood JP, McCann GP, et al. Magnetic resonance perfusion or fractional flow reserve in coronary disease. *N Engl J Med* 2019;380(25):2418-2428.
50. Garcia MJ, Kwong RY, Scherrer-Crosbie M, et al. State of the art: Imaging for myocardial viability: A scientific statement from the American Heart Association. *Circ Cardiovasc Imaging* 2020;13(7):e000053.
51. Delaney FT, Dempsey P, Welaratne I, Buckley B, O'Sullivan D, O'Connell M. Incidental cardiac uptake in bone scintigraphy: Increased importance and association with cardiac amyloidosis. *BJR Case Rep* 2021;7(3):20200161.
52. Kratochwil C, Flechsig P, Lindner T, et al. (68)Ga-FAPI PET/CT: Tracer uptake in 28 different kinds of cancer. *J Nucl Med* 2019;60(6):801-805.
53. Heckmann MB, Reinhardt F, Finke D, et al. Relationship between cardiac fibroblast activation protein activity by positron emission tomography and cardiovascular disease. *Circ Cardiovasc Imaging* 2020;13(9):e010628.
54. Wu M, Ning J, Li J, et al. Feasibility of in vivo imaging of fibroblast activation protein in human arterial walls. *J Nucl Med* 2022;63:948-951.
55. Tzolos E, Bing R, Andrews J, et al. In vivo coronary artery thrombus imaging with 18F-GP1 PET-CT. *Eur Heart J* 2021;42(Suppl. 1):ehab724.0261.
56. Velangi PS, Choo C, Chen K-HA, et al. Long-term embolic outcomes after detection of left ventricular thrombus by late gadolinium enhancement cardiovascular magnetic resonance imaging: A matched cohort study. *Circ Cardiovasc Imaging* 2019;12(11):e009723.
57. Kwiecinski J, Cadet S, Daghem M, et al. Whole-vessel coronary 18F-sodium fluoride PET for assessment of the global coronary microcalcification burden. *Eur J Nucl Med Mol Imaging* 2020;47(7):1736-1745.
58. Brendle C, Schmidt H, Oergel A, et al. Segmentation-based attenuation correction in positron emission tomography/magnetic resonance. *Invest Radiol* 2015;50(5):339-346.
59. Freitag MT, Fenchel M, Bäumer P, et al. Improved clinical workflow for simultaneous whole-body PET/MRI using high-resolution CAIPRINHA-accelerated MR-based attenuation correction. *Eur J Radiol* 2017;96:12-20.
60. Arabi H, Zaidi H. MRI-guided attenuation correction in torso PET/MRI: Assessment of segmentation-, atlas-, and deep learning-based approaches in the presence of outliers. *Magn Reson Med* 2022;87(2):686-701.
61. Armstrong IS, Tonge CM, Arumugam P. Assessing time-of-flight signal-to-noise ratio gains within the myocardium and subsequent reductions in administered activity in cardiac PET studies. *J Nucl Cardiol* 2019;26(2):405-412.
62. Robson PM, Trivieri MG, Karakatsanis NA, et al. Correction of respiratory and cardiac motion in cardiac PET/MR using MR-based motion modeling. *Phys Med Biol* 2018;63(22):225011.
63. Petibon Y, Sun T, Han PK, Ma C, El FG, Ouyang J. MR-based cardiac and respiratory motion correction of PET: Application to static and dynamic cardiac 18F-FDG imaging. *Phys Med Biol* 2019;64(19):195009.
64. Lassen ML, Rasul S, Beitzke D, et al. Assessment of attenuation correction for myocardial PET imaging using combined PET/MRI. *J Nucl Cardiol* 2019;26(4):1107-1118.
65. Tarkin JM, Joshi FR, Evans NR, et al. Detection of atherosclerotic inflammation by 68Ga-DOTATATE PET compared to [18F]FDG PET imaging. *J Am Coll Cardiol* 2017;69(14):1774-1791.
66. Tarkin JM, Calcagno C, Dweck MR, et al. (68)Ga-DOTATATE PET identifies residual myocardial inflammation and bone marrow activation after myocardial infarction. *J Am Coll Cardiol* 2019;73:2489-2491.
67. Jenkins WSA, Vesey AT, Stirrat C, et al. Cardiac  $\alpha V\beta 3$  integrin expression following acute myocardial infarction in humans. *Heart* 2017;103(8):607-615.